IEEE Access
Multidisciplinary | Rapid Review | Open Access Journal

Received June 1, 2019, accepted June 17, 2019, date of publication June 26, 2019, date of current version July 15, 2019.

Digital Object Identifier 10.1109/ACCESS.2019.2925064

Active Current Sharing of a Parallel DC-DC Converters System Using Bat Algorithm Optimized Two-DOF PID Control

SYUAN-YI CHEN[1], BO-CHEN YANG[2], TSE-AN PU[1], CHIH-HUNG CHANG[1], AND RUEI-CING LIN[1]

[1]Department of Electrical Engineering, National Taiwan Normal University, Taipei 106, Taiwan
[2]Power Design Department I, Wistron Corporation, Taipei 114, Taiwan

Corresponding author: Syuan-Yi Chen (chensy@ntnu.edu.tw)

This work was supported by the Ministry of Science and Technology, Taiwan, under Grant MOST 107-2221-E-003-016.

ABSTRACT This paper presents a current sharing method to actively balance the output currents of a parallel dc–dc converters' (PDCC) system regarding the demanded power. First, the operating principle of the PDCC system with parallel-connected bidirectional converters is studied. To regulate the output voltage in dc bus and share the output currents of the individual converters, a dual-loop control architecture comprising an outer voltage control loop and multiple inner current control loops is designed based on the automatic master–slave control scheme. Moreover, a feedback-type two-degree-of-freedom proportional-integral-derivative (FB2PID) controller is introduced to obtain the pulse-width modulation control signals for the converters. In order to improve the dynamic response and robustness of the active current-sharing control performances of the FB2PID controlled PDCC system, a bat algorithm (BA)-optimized FB2PID control system is further proposed to concurrently and dynamically optimize the control parameters of the FB2PID controller in the current control loop. Thus, the output current of each converter can be controlled to share the demand power equally in the presence of uncertainties. Finally, the simulation and experimental results reveal that the proposed BA-optimized FB2PID control system outperforms the conventional PID and FB2PID control systems with regard to the voltage regulation and current sharing performances under the time-varying electric load condition.

INDEX TERMS Bat algorithm, current sharing, parallel dc–dc converters system, optimization, two degree-of-freedom proportional-integral-derivative control.

I. INTRODUCTION

With the advances in renewable energy and distributed power system, the requirements of high power systems are getting increasingly. In this aspect, a parallel DC–DC converters (PDCC) system is a good alternative to increase output power level and to provide high reliability and steady current output [1], [2]. To date, PDCC systems have seen popularly applied in many distributed power systems due to their benefits over a single stand-alone unit in reliability, reconfigurability, cost, efficiency, fault tolerance, power processing capability, redundancy and modular architecture [1]–[6]. Though the specifications of the all converters could be the same, the differences of their external power sources and internal converter parameters result in the different output currents.

The most common current-sharing technique is the open-loop droop method, which independently regulates the output impedance or the voltage of the converter to realize uniform current distribution among the parallel-connected converters [7]. However, the droop control method may cause unbalanced current sharing and improper voltage variation due to the presence of droop and line resistance between converters [7]–[9]. Thus, some techniques have been developed to improve the conventional droop control such as primary droop control [10], improved droop control [11], [12], adaptive droop control [13], [14], generalized droop control [15],

The associate editor coordinating the review of this manuscript and approving it for publication was Yanbo Chen.

and closed-loop droop control [16]. Another widely used method for paralleling schemes is the active current sharing method (ACSC) based on its good control performance, modularity and simplicity [3]–[5]. Four most common schemes used for ACSC are the average current control, master-slave control with dedicated master, master-slave control with rotating master, and master-slave control with automatic master [12], [17]. In these methods, slave modules are controlled via the current-sharing bus and closed-loop controller such that their output currents can track the reference current more accurately as compared to the droop control. As a result, all the converters share the demanded load current equally and thus the PDCC system can be considered as a multi-input and single-output power supply system. However, if the current-sharing bus or the controller fails, the reliabilities and functionalities of the whole system will be destroyed.

To improve the reliability of the system, some new master-slave control schemes have been raised such as masterless modular current-sharing technique [18] and wireless master-slave communication interfaces [3], [4]. On the other hand, some advanced control strategies were also recently proposed to improve the control performances and robustness of the master-slave based ACSC methods in the literatures. In [5], a proportional-integral (PI) sliding mode controller was designed to control a parallel buck converters system. The sliding surface consisting of current error, voltage error, and the integral of both errors was introduced to reduce the both errors and to improve the robustness of the system. In [6], a finite-time ACSC algorithm was designed for a parallel buck converters system. It showed that not only the output voltage of the system can reach the reference voltage in a finite time, but also the objective of current sharing can be achieved within almost the same time. In [8], a new ACSC method was proposed for a switch power supply where only the maximum and minimum currents of the power modules were regulated. Moreover, a fuzzy gain scheduling of PI controller was used to compensate for the output voltage error of a parallel-connected converter system in [19]. The fuzzy method obtains tight output voltage regulation and current control performances in both the steady-state operation and the transient response. Furthermore, a parallel fuel cell generation system was presented in [20]. In [20], a master-slave model predictive control with neural network optimization was developed for the ACSC object. In addition, a genetic algorithm (GA) tuned PID control system was developed to control a parallel buck converters system in [21]. In the present study, a novel control with optimization strategy, different from these aforementioned methods, was developed.

In many industrial and academic control applications, proportional-integral-derivative (PID) control is the mostly preferred method due to its simple control structure, clear physical meaning, and easy implementation [22]–[24]. To obtain favorable control performances for the PID controller, tuning control parameters including proportional (P) gain, integral (I) gain, and derivative (D) gain is the main task. Classical design techniques such as Ziegler–Nichols and Cohen–Coon tuning methods can be applied to determine the appropriate values for these control parameters. However, these methods usually take long time and trivial procedures to get the optimal values for specific control situations. On the other hand, there is only one tunable element in the closed-loop transfer function from the set-point variable to the controlled variable and that from the external disturbance to the controlled variable in the conventional PID control system. Since the degree-of-freedom (DOF) of a control system is defined as the number of closed-loop transfer functions that can be independently adjusted, this fact indicates that the tracking and disturbance rejection abilities cannot be concurrently optimized by using the conventional one DOF PID (1PID) controller [25]. If the disturbance response is optimized, the tracking response could be poor, and vice versa. To resolve this disadvantage, a two DOF PID (2PID) control system was proposed by integrating an additional compensation loop [25], [26]. In contrast to the 1PID controller with only one tunable element, the main advantages of the 2PID controller over 1PID controller is the possibility of decoupling set-point and external disturbance signals so that the tracking response and disturbance rejection ability can be simultaneously improved.

Though the 2PID controller can improve the control performances of the 1PID controller, it is difficult to ensure the system stability and control precision in the presences of plant uncertainties and external disturbances due to its linear structure and constant control gains. To improve the robustness and adaptiveness of the 2PID control system, the control parameters including three main parameters, namely the P gain (K_P), I time constant (T_I), and D time constant (T_D) with two compensation parameters, namely the P compensation constant (α) and D compensation constant (β) should be dynamically adjusted during the control process. However, finding and tuning these control gains are complicated optimization problems. At present, several strategies were proposed to tune these control parameters automatically such as the simple method [27], robust tuning [28], and evolutionary algorithms (EAs) [25], [29]–[31].

Optimization in real-world applications usually involves many design variables and complicated constraints [32], [33]. The objective of an optimization problem can usually be regarded as the minimization of cost and time, or maximization of benefit and performance. Recently, the optimization using EA-based approaches has gained increasing attention due to their easy structure and superior optimization performance. In general, these approaches are naturally inspired by two aspects in the real world [22], [34]. The first one is Darwin's theory which indicates only the more adapted individuals can survive in an unforgiving struggle for existence. In this class of EAs, the better solutions, generated by using specific operations such as crossover, selection, and mutation, can survive and evolve their values in the next generation. Both GA and differential evolution are the frequently used ones. The second concept is based on social behaviors of individuals in a swarm [33]. In this class of EAs, the

biological swarms such as bees, bats, birds, fireflies, and ants are randomly generated and continuously moved within a search space using some variation operators. To date, several swarm intelligence algorithms have been proposed such as artificial bee colony algorithm [25], bat algorithm (BA) [32], [34]–[42], particle swarm optimization [43], firefly algorithm (FA) [44], and ant colony optimization [45].

BA is one of EAs inspired by the natural echolocation behavior of bat swarm in searching for the prey. The echolocation behavior of bat involves local search through random walks and global exploration. When flying and hunting, bats emit a very loud sound pulse and listen for the echo that bounces back from the surrounding objects [32], [35], [41]. The pulses of the echolocation vary in properties and can be in connection with hunting strategies, depending on the species. On the other hand, the loudness also varies from the loudest when searching for the prey and to the quietest when approaching the prey. Studies indicate that the information from the echoes will enable bats to build up three dimensional scenarios of their surroundings for accurately determining the distance, orientation, and even the moving speed of the prey. In addition, bats are able to discriminate different types of insects through the variations of the Doppler effect even in the presence of complete darkness. According to the intelligence of bat swarm, the BAs comprises the advantages over other swarm based intelligent algorithms such as fewer mathematical requirement, automatic search space zoom out capability, and automatic transfer from exploration to exploitation mechanism [36]. Therefore, it has been successfully applied to a wide variety of real world applications such as digital signal processing [37], image classification [38], robot control [39], price estimation [40], trajectory planning [41], and power forecasting [42].

The motivation of this study was to develop a high precision and robust ACSC scheme to solve the output current imbalance problem of the PDCC system. Although the current sharing among the parallel-connected converters can be controlled through an external controller, designing control parameters for the controller in advance is difficult in practical applications. They should always be adjusted through trial-and-error procedures when the control performance degrades. Moreover, the current-sharing control with constant control parameters cannot ensure the robustness in the presences of converter uncertainties, load changes, and external disturbances. To cope with the disadvantages as aforementioned, a feedback type 2PID (FB2PID) control system with favorable tracking and disturbance rejection abilities was firstly adopted to regulate the output voltage of the PDCC system and the output current of each converter for equally sharing the load current. To improve the robustness of the FB2PID control system, a BA optimization method was further used to dynamically and concurrently tune the control parameters of the FB2PID controllers in the current control loop. As a result, the control parameters can be effectively tuned without the need of trivial trials. Simulations and experiments were conducted to verify the effectiveness and performances of the proposed BA-optimized FB2PID control system. The contributions of this study are summarized as follows:

1) Development of a PDCC system with parallel-connected bidirectional buck-boost converters: A PDCC system with three parallel-connected bidirectional buck-boost converters and one external DSP controller was successfully developed. Compared with the existing PDCC systems, which can be only operated in buck or boost mode with single power transferring direction [5], [6], [9], [10], [21], the developed PDCC system provides dual power transferring directions and is available for both boost and buck modes.
2) Design of a new BA-optimized FB2PID control system: In this study, a new BA-optimized FB2PID control system that benefits from FB2PID control and online optimization was proposed. In this controller, an additional feedback control path is able to simultaneously improve the control precision and disturbance rejection ability of the conventional PID control. On the other hand, five control parameters were dynamically and concurrently optimized according to the BA so that the robustness of the control system can be improved while the trivial trials for the control parameters are not necessary.
3) Practical application of online optimization for the control of a PDCC system: To date, only a few researches used evolutionary algorithms to online optimize the controller of PDCC system [21]. In this study, a BA was adopted to online tune the control parameters in the inner current control loop. Voltage regulation, current control, online optimization, and automatic master-slave control mechanism were integrated and realized through a single DSP controller. The successful real-time implementation implied that the proposed BA-optimized FB2PID control strategy is feasible to the online ACSC in practical PDCC applications.
4) Simulation and experiment comparisons for three control strategies under time-varying electric load condition: Both simulation and practical experimental tests were conducted to compare the voltage regulation and current sharing performances of the PID, FB2PID, and BA-optimized FB2PID control systems. Compared with the conventional PID control, evident voltage regulation and current sharing improvements obtained by the proposed BA-optimized FB2PID control system were confirmed through both simulation and experiment.

The rest of this study is organized as follows: the operating principle of the PDCC system is presented in Section II; the details of the BA is introduced in Section III; the ACSC mechanism using the proposed BA-optimized FB2PID control system with automatic master-slave method are described in Section IV; numerical simulation and experimentation are discussed in Sections V and VI, respectively; and the conclusions are given in Section VII.

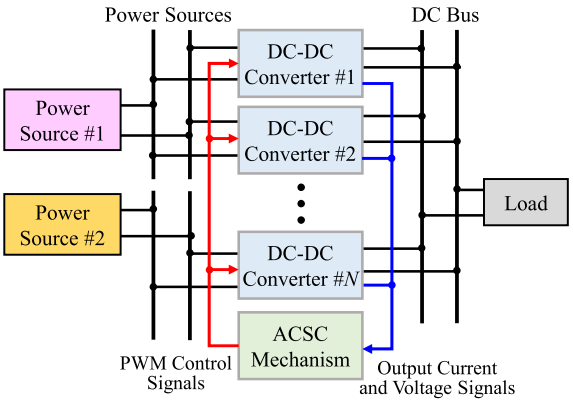

FIGURE 1. Block diagram of the PDCC system with ACSC mechanism.

II. PARALLEL DC-DC CONVERTERS SYSTEM

A typical PDCC system connecting a number of N DC-DC converters in parallel is illustrated by **FIGURE 1**. Each DC-DC converter connecting to specific power source can be operated either stand-alone or in parallel to perform high power output and fulfill the requirements of demanded load current. In this study, the ACSC mechanism is designed based on the automatic master-slave method to monitor the difference between the reference current and the output (or inductor) current of each converter. The difference information is incorporated into the control loop so that the output currents of the converters can be managed to share the stress and the load current of the whole PDCC system.

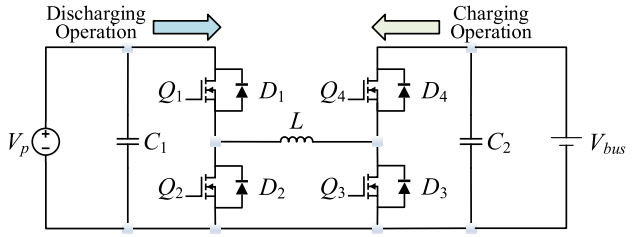

FIGURE 2. Configuration of the bidirectional DC-DC converter.

A. CONFIGURATION OF SINGLE DC-DC CONVERTER

The topology of the adopted bidirectional DC-DC converter is composed of an inductor L, two capacitors $C_{1,2}$, four diodes $D_{1\sim4}$, and four power switches $Q_{1\sim4}$, as shown in **FIGURE 2** [46]. It is capable of operating in all power transferring directions. By comparing the power source voltage (V_p) and the DC bus voltage (V_{bus}), buck or boost mode can be determined. If a chargeable battery is adopted as the power source, charging/discharging operation is accordingly defined as that the energy is transferred from the DC bus/power source to the power source/DC bus. In addition, since the power source voltage may be higher or lower than the DC bus voltage, boost-charging, buck-charging, boost-discharging and buck-discharging modes can be further achieved by adequately controlling the power switches $Q_{1\sim4}$.

TABLE 1. Four modes under discharging and charging operations.

Operation Mode	$V_p > V_{bus}$	$V_p < V_{bus}$
Discharging operation (Q_2: off, Q_4: off)	Buck-discharging: Q_1: control, Q_3: off	Boost-discharging: Q_1: on, Q_3: control
Charging operation (Q_1: off, Q_3: off)	Boost-charging: Q_2: control, Q_4: on	Buck-charging: Q_2: off, Q_4: control

The corresponding control signals of power switches with respect to each operation mode are summarized in Table 1. As such, the power flow and energy transfer can be well controlled for the four operation modes.

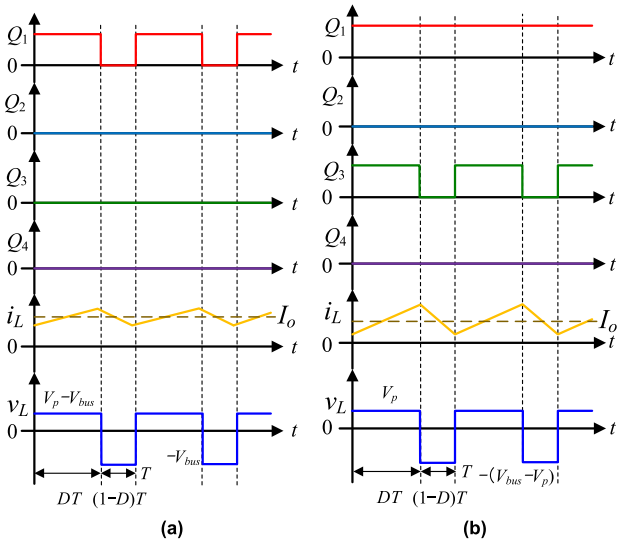

FIGURE 3. The waveforms of the switch statuses and inductor current during discharging operation: (a) buck-discharging mode, (b) boost-discharging mode.

B. MODE ANALYSIS OF DC-DC CONVERTER

In this study, the buck-discharging and boost-discharging modes are selected to explain the operating principle of the ACSC mechanism. The other two operation modes can be analyzed through the same concept. The waveforms of the switch statuses and inductor current during the discharging operation are shown in **FIGURE 3.** If V_p is higher than V_{bus}, the converter is operated at buck-discharging mode. During this mode, the power switch Q_1 is switched while $Q_{2\sim4}$ are turned off to regulate the inductor current i_L as shown in **FIGURE 3**(a). In the first time interval ($0 < t < DT$) of period T where D is a duty cycle, $0 < D < 1$, the power switch Q_1 is turned on so that the equivalent circuit of the DC-DC converter can be expressed as **FIGURE 4**(a). At this time, the voltage across the inductor v_L equals to the difference of the power source voltage V_p and the DC bus voltage V_{bus}, namely $v_L = V_p - V_{bus}$. Since V_p is higher than V_{bus} in buck-discharging mode, the voltage v_L is positive which means that the inductor current i_L increases linearly with

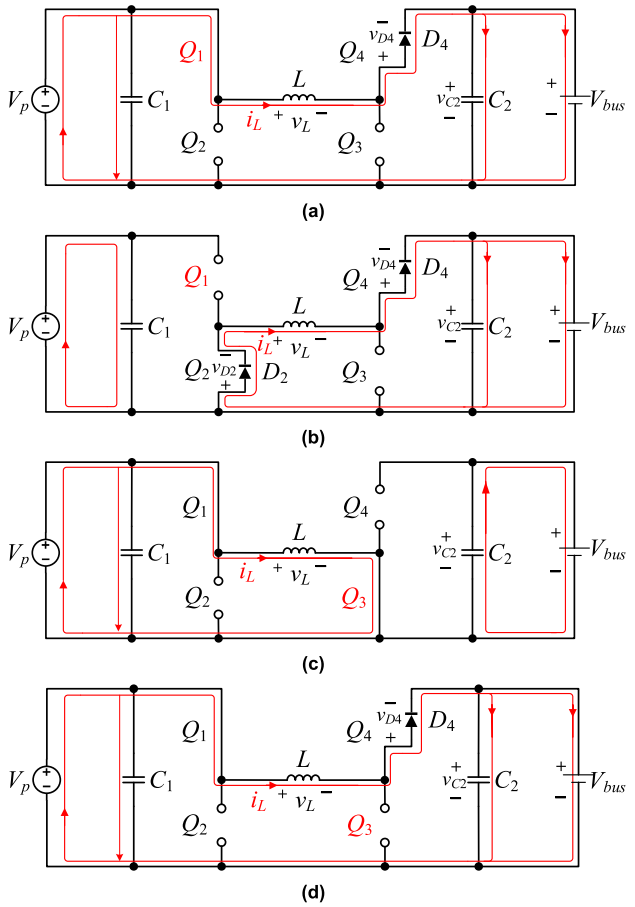

FIGURE 4. Equivalent circuits of different switch statuses. (a) The first time interval ($0 < t < DT$ during buck-discharging mode. (b) The second time interval $DT < t < T$ during buck-discharging mode. (c) The first time interval ($0 < t < DT$ during boost-discharging mode. (d) The second time interval $DT < t < T$ during boost-discharging mode.

a smaller slope as follows:

$$i_L(t) = i_L(0) + \frac{1}{L}\int_0^t v_L\, d\tau = i_L(0) + \frac{1}{L}(V_p - V_{bus})\, t \quad (1)$$

The power source supplies the power to the load through power switch Q_1, inductor L, and diode D_4. Moreover, the inductor current i_L at $t = DT$ is:

$$i_L(DT) = i_L(0) + \frac{1}{L}(V_p - V_{bus})\, DT \quad (2)$$

In the second time interval ($DT < t < T$), the power switch Q_1 is turned off so that the equivalent circuit is expressed as as **FIGURE 4**(b). At this time interval, $v_L = -V_{bus}$, the inductor current i_L can be derived as follows:

$$i_L(t) = i_L(DT) + \frac{1}{L}\int_{DT}^t v_L d\tau = i_L(DT) - \frac{V_{bus}}{L}(t - DT) \quad (3)$$

At this time interval, the inductor L supplies the power to the load through diodes D_2 and D_4. As seen from (3), the inductor current i_L at $t = T$ is:

$$i_L(T) = i_L(DT) - \frac{V_{bus}}{L}(1 - D)T \quad (4)$$

Hence, substituting (2) to (4) obtains the inductor current i_L in steady-state as below:

$$i_L(T) = i_L(0) + \frac{1}{L}(V_p - V_{bus})DT - \frac{V_{bus}}{L}(1 - D)T \quad (5)$$

Because $i_L(T) = i_L(0)$, the ratio of V_{bus} and V_p is derived via (5):

$$\frac{V_{bus}}{V_p} = D \quad (6)$$

which indicates that the converter is operated in a buck mode.

The converter is operated at boost-discharging mode if V_p is lower than V_{bus}. During this mode, the power switch Q_3 is switched, Q_1 is turned on, and Q_2 and Q_4 are turned off to regulate the inductor current i_L as shown in **FIGURE 3**(b). In the first time interval ($0 < t < DT$), the switch Q_3 is turned on so that the equivalent circuit is expressed as **FIGURE 4**(c). At this time, $v_L = V_p$, the inductor current i_L is obtained as follows:

$$i_L(t) = i_L(0) + \frac{1}{L}\int_0^t v_L\, d\tau = i_L(0) + \frac{1}{L}V_p\, t \quad (7)$$

Hence, the load power is supplied by the capacitor C_2 solely. Moreover, the inductor current i_L at $t = DT$ is:

$$i_L(DT) = i_L(0) + \frac{1}{L}V_p\, DT \quad (8)$$

In the second time interval ($DT < t < T$), the power switch Q_3 is turned off and the corresponding equivalent circuit is expressed as III(d). At this time interval, $v_L = -(V_{bus} - V_p)$, the inductor current i_L can be derived as follows:

$$i_L(t) = i_L(DT) + \frac{1}{L}\int_{DT}^t v_L d\tau = i_L(DT) + \frac{1}{L}[-(V_{bus} - V_p)](t - DT) \quad (9)$$

At this time interval, the inductor L supplies the power to the load through diode D_4. The inductor current i_L at $t = T$ is:

$$i_L(T) = i_L(DT) + \frac{1}{L}[-(V_{bus} - V_p)](1 - D)T \quad (10)$$

Similarly, the inductor current i_L in the steady-state can be formulated using (8) and (10) as below:

$$i_L(T) = i_L(0) + \frac{1}{L}V_p DT + \frac{1}{L}[-(V_{bus} - V_p)](1 - D)T \quad (11)$$

Because $i_L(T) = i_L(0)$, the ratio of V_{bus} and V_p is derived from (11) as follows:

$$\frac{V_{bus}}{V_p} = \frac{1}{1 - D} \quad (12)$$

The result indicates that the converter is operated in a boost mode. According to the same operating concept, the boost-charging and buck-charging operation modes can be realized

by controlling the power switches Q_2 and Q_4 while Q_1 and Q_3 are turned off, as given in Table 1.

III. BAT ALGORITHM

BA is a heuristic optimization algorithm inspired by the echolocation behavior of bat swarm in searching for the prey. In the beginning of the BA, the bat blindly flies around the search space as well as emits sound wave with specified loudness A and pulse emission rate γ. Then, the bat receives feedback signals with the inclusion of its own signal and possibly signals from other bats by echolocation. If the loudness and pulse emission rate of the received signal are strong and low, respectively, it indicates that the bat becomes closer to its prey. Therefore, the bat decreases the loudness as well as increases the pulse emission rate. Conversely, if the loudness and pulse emission rate of the received signal are weak and high, respectively, the bat continues its blind flight with the same intensity of the emitted sound wave. As such, bats are able to use the time delay information of the received signals to build up three dimensional scenario of the surrounding.

In the BA, each bat adjusts its position to find the prey in a D-dimensional space. The position $\mathbf{x}_i^t$ and velocity $\mathbf{v}_i^t$ of the ith bat at the tth iteration is updated through the following equations [32], [34]–[42]:

$$\mathbf{v}_i^t = \mathbf{v}_i^{t-1} + (\mathbf{x}_i^t - \mathbf{x}^*)f_i \tag{13}$$

$$\mathbf{x}_i^t = \mathbf{x}_i^{t-1} + \mathbf{v}_i^t \tag{14}$$

where $i = 1, 2, \ldots P$, in which P is the population size; $\mathbf{x}^*$ is the current global best solution among the all bats; f_i is the frequency of the ith bat's echolocation, which is generated in the range $[f_{\min} \quad f_{\max}]$ and updated in every iterations follows:

$$f_i = f_{\min} + (f_{\max} - f_{\min})\rho \tag{15}$$

where $\rho \in [0, 1]$ is a random value drawn from a uniform distribution. According to (13)–(15), each bat adjusts its position according to the time-varying frequency and velocity. Moreover, if there are no detected preys, an additional random fly is used in order to explore the new search area by the following equation:

$$\mathbf{x}_{\text{new}} = \mathbf{x}^* + \varepsilon A^t \tag{16}$$

where $\varepsilon \in [-1, 1]$ is a random value, $A^t =< A_t^i >$ is the average loudness of the all bats allowing the bats to perform an enhanced global exploration of its space.

The value of loudness A_i is decreased while the value of the pulse emission rate γ_i is increased during the time iterations via the equations as shown in the following:

$$A_i^{t+1} = \varphi A_i^t \tag{17}$$

$$\gamma_i^{t+1} = \gamma_i^0 \left[1 - e^{-\lambda t}\right] \tag{18}$$

where φ and λ are the decreasing and increasing coefficients satisfying the conditions $0 < \varphi < 1$ and $\lambda > 0$, respectively; γ_i^0 is the initial pulse emission rate. Thus, the following results can be obtained:

$$A_i^t \to 0, \gamma_i^t \to \gamma_i^0, as\, t \to \infty. \tag{19}$$

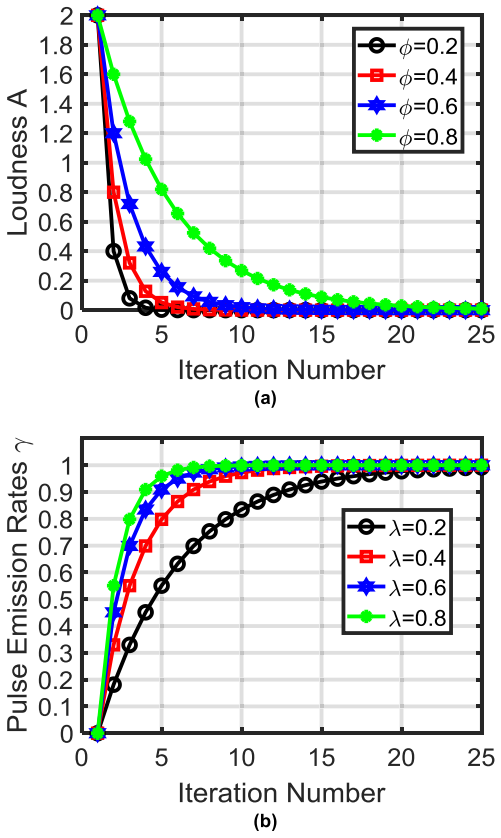

FIGURE 5. Iterative evolutions of loudness and pulse emission rate for 25 iterations: (a) changes of loudness and (b) changes of pulse emission rate.

If the initial values of the loudness A and pulse emission rate γ are set as 2 and 1, respectively, their changes with different coefficients φ and λ can be seen in **FIGURE 5**. Finally, the termination criterion of the BA is normally related to computational time constraint, generation iteration number, or quality of the final outcomes.

IV. ACSC USING BA-OPTIMIZED FB2PID CONTROL SYSTEM

A. ACSC WITH AUTOMATIC MASTER-SLAVE METHOD

To concurrently control the DC bus voltage of the whole PDCC system and the output current of each converter, the ACSC with automatic master-slave method is developed, which contains an outer voltage control loop and multiple inner current control loops as illustrated in **FIGURE 6**. For the voltage control loop, the voltage control error e_V is determined as $e_V = V_{ref} - V_o$ where V_{ref} and V_o represent the reference and actual DC bus voltages, respectively; k indicates the kth converter. The output of voltage controller is a compensation signal i for the current loop. Hence, the automatic master-slave method is adopted so that the highest output current among the all converters is regarded as the reference current i_{ref} for the rest ones as follows:

$$i_{ref} = \max(i_{o1}, i_{o2}, \ldots i_{oN}) \tag{20}$$

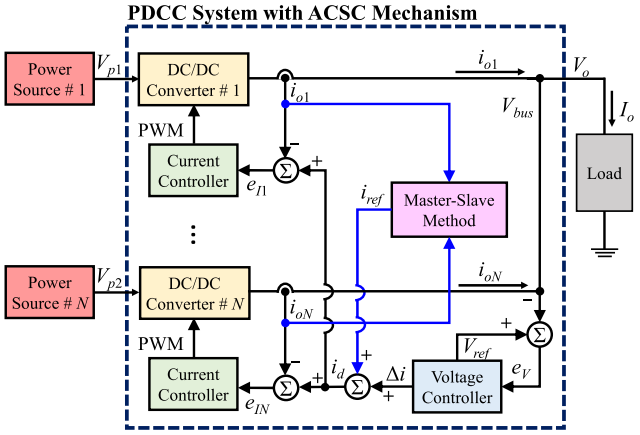

FIGURE 6. ACSC mechanism of a PDCC system using automatic master-slave control method.

where N is the number of the parallel-connected converters, i_{ok} is the output current of the kth converter. The modified current demand i_d is obtained by adding the reference current i_{ref} and the compensation signal i. As a result, the current control error e_{Ik} can be determined by comparing the actual output current i_{ok} and current demand i_d as $e_{Ik} = i_d - i_{ok}$. Finally, the pulse width modulation (PWM) control signal can be determined by using the current controller with respect to the current error e_{Ik}. In this regard, all the converters can output the equivalent currents under the same DC bus voltage to provide higher power that the load requires.

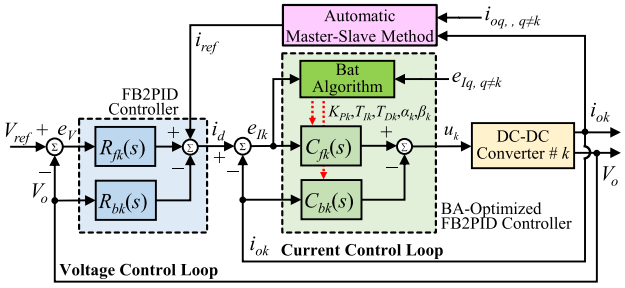

FIGURE 7. Control diagram of the BA-optimized FB2PID control system.

B. ACSC USING FB2PID CONTROL SYSTEM

In this study, the voltage and current control loops are all controlled by the FB2PID controllers. In contrast to the conventional 1PID controller with an only feedforward control path $C_f(s)$, a feedback control path $C_b(s)$ is added to the FB2PID controller to simultaneously improve the control precision and disturbance rejection ability as illustrated in **FIGURE 7**. The transfer functions $C_{fk}(s)$ and $C_{bk}(s)$ of the FB2PID controller in the k_{th} inner current control loop are formulated as follows [31]:

$$C_{fk}(s) = K_{Pk}\left((1-\alpha_k) + \frac{1}{T_{Ik}s} + (1-\beta_k)T_{Dk}F(s)\right) \quad (21)$$

$$C_{bk}(s) = K_{Pk}\left(\alpha_k + \beta_k T_{Dk}F(s)\right) \quad (22)$$

where K_{Pk}, T_{Ik}, and T_{Dk} denote the main parameters corresponding to the P gain, I, and D time constants, respectively; $0 \le \alpha_k \le 1$ and $0 \le \beta_k \le 1$ denote additional compensation P and D parameters, respectively; $F(s)$ is a derivative filter defined as $F(s) = s/(1+\tau s)$ where τ is a time constant. Thus, the final PWM control signal $u_k(s)$ can be obtained by using (21)–(22) as follows:

$$u_k(s) = K_{Pk}\left\{\left[(1-\alpha_k) + \frac{1}{T_{Ik}s} + (1-\beta_k)T_{Dk}\frac{s}{1+\tau s}\right]e_{Ik} - \left[\alpha_k + \beta_k T_{Dk}\frac{s}{1+\tau s}\right]i_{ok}\right\} \quad (23)$$

Moreover, the transfer functions $R_{fk}(s)$ and $R_{bk}(s)$ of the FB2PID controller in the outer voltage control loop can also be formulated by (21)–(22) via the same concept. Though the FB2PID controller is able to improve the tracking response of the conventional 1PID controller with respect to the well-designed compensation path [25], it is necessary to manually adjust a control parameter set $\{K_{Pk}, T_{Ik}, T_{Dk}, \alpha_k, \beta_k\}$ for achieving the best control performance. Because of the complicated coupling between the parameters, it is difficult to determine these parameters perfectly by trial-and-error. In addition, the robustness of the PDCC system cannot be ensured by using the FB2PID controllers with constant control gains.

C. ACSC USING BA-OPTIMIZED FB2PID CONTROLLER

To improve the response speed and robustness of the ACSC mechanism in the presences of plant uncertainties and external disturbances, the BA is further adopted to tune the control parameter set $\{K_{Pk}, T_{Ik}, T_{Dk}, \alpha_k, \beta_k\}$ in the current control loop as shown in **FIGURE 7**. In this control scheme, each bat is formulated as a solution vector $\mathbf{x}_i$, namely $\mathbf{x}_i = [K_{P1}, T_{I1}, T_{D1}, \alpha_1, \beta_1, \ldots, K_{PN}, T_{IN}, T_{DN}, \alpha_N, \beta_N] \in \Re^{1\times 5N}$, to optimize the control parameters of N current controllers with respect to the N converters. Each bat is randomly generated within the specific searching ranges. After that, the vector $\mathbf{x}_i$ is applied to a number of N FB2PID current controllers. Hence, an integral of time multiplying the absolute value of the error (ITAE) is chosen as a performance index J_i to evaluate the ACSC in the following:

$$J_i(\mathbf{x}_i) = \sum_{t=t_1}^{t_2} t\left(\sum_{k=1}^{N} |\, e_{Ik}(\mathbf{x}_i, t)\,|\right)dt \quad (24)$$

where t_1 and t_2 represent a time period used to complete a parameter optimization process. Finally, the vector x^* obtaining the highest fitness value fit_i is memorized as the optimal solution for the practical PDCC system as follows:

$$\text{Find } \mathbf{x}_i \text{ which maximizes } fit_i(\mathbf{x}_i) = \frac{1}{\eta + J_i(\mathbf{x}_i)} \quad (25)$$

where η denotes a small positive constant. All the BA operations are repeated until the optimal fitness value is achieved or a preset count of the generation number is reached. Thus, the control parameters of the BA-optimized

FB2PID control system are auto-tuning to minimize the current control errors resulted in the all converters.

For the BA, adjustments of the parameters φ and λ significantly affect the convergence time in updating controller parameters. In addition, the pre-defined small iteration number and population size, and a simple stopping condition of the BA will result in short convergence time. With the help of short convergence time, the control parameters of the FB2PID controllers can be tuned by a high update rate to achieve good transient response for the PDCC system. However, they may also engender undesired oscillations in steady-state response. On the contrary, the convergence time of the BA is long if the iteration number and population size are big as well as the stopping condition is hard. Thus, the update rate is low while the whole control response is relatively stable. However, the obtained optimal solutions may not be the current best control parameters due to the variant computational time difference. To this end, all the parameters of the BA should be appropriately set by some trials to balance the execution speed, optimization efficiency and system stability.

V. SIMULATION RESULTS

In the simulation, three bidirectional DC–DC converters are connected in parallel for investigation. The input voltages of the converters were set as 40V with random voltage vibrations within ±5V. The output voltage was set as 48V. Thus, the PDCC system was operated at a boost-discharging mode. Moreover, the output currents of individual converters were simulated under a time-varying demanded power, which steps from 21 to 9A at 0.2 second and 9 to 21A at 0.3 second, respectively.

A. PERFORMANCE MEASURES

To investigate the ACSC performance and robustness of the PDCC system using the proposed BA-optimized FB2PID controller, a conventional 1PID controller was also used to control the outer voltage and inner current control loops for comparison. The feedforward control path $C_k(s)$ of the adopted 1PID controller can be formulated as follows:

$$C_k(s) = K_{Pk}\left(1 + \frac{1}{T_{Ik}s} + T_{Dk}D(s)\right) \tag{26}$$

In the simulation, the performance measures including maximum voltage control error P_{VM}, average voltage control error P_{VA}, and standard deviation of the voltage control error P_{VS} in the DC bus were determined for comparison with the values obtained from the 1PID, FB2PID, and the proposed BA-optimized FB2PID control systems as follows:

$$P_{VM} = \max_{I}\left(|e_V(I)|\right) \tag{27}$$

$$P_{VA} = \frac{\sum_{I=1}^{R}|e_V(I)|}{R} \tag{28}$$

$$P_{VS} = \sqrt{\sum_{I=1}^{R}\frac{(|e_V(I)| - P_{VA})^2}{R}} \tag{29}$$

where I is the iteration number; R is the number of total iterations during the control process. To evaluate the ACSC performance of the parallel-connected converter, a current control error rate E_k is firstly defined as follows:

$$E_k(I) = \frac{i_{ok}(I) - \sum_{k=1}^{N}\frac{i_{ok}(I)}{N}}{\sum_{k=1}^{N}\frac{i_{ok}(I)}{N}}. \tag{30}$$

Thus, the maximum current control error rate P_{IM}, average current control error rate P_{IA}, and standard deviation of the current control error rate P_{IS} can be measured for comparison as follows:

$$P_{IM} = \max_{k}\max_{I}\left(|E_k(I)|\right) \tag{31}$$

$$P_{IA} = \frac{\sum_{k=1}^{N}\sum_{I=1}^{R}|E_k(I)|}{N \times R} \tag{32}$$

$$P_{IS} = \frac{\sum_{k=1}^{N}\sqrt{\sum_{I=1}^{R}\frac{(|E_k(I)| - P_{IA})^2}{R}}}{N}. \tag{33}$$

The ACSC performances of the PDCC system can be compared using P_{VM}, P_{VA}, P_{IM} and P_{IA}. The stability of the control response can be observed via the P_{VS} and P_{IS}.

B. RESULTS

In this study, the simulation was completed by using PSIM with C block software. The constant parameters for the 1PID control system in the voltage and current control loops were chosen as $K_P = 30$, $T_I = 0.02$, and $T_D = 0.1$, and $K_P = 8$, $T_I = 0.14$, and $T_D = 0.1$, respectively. Besides, the constant parameters for the FB2PID control system in the voltage and current control loops were chosen as $K_P = 35$, $T_I = 0.026$, $T_D = 0.2$, $\alpha = 0.09$, and $\beta = 0.05$, and $K_P = 8.2$, $T_I = 0.15$, $T_D = 0.2$, $\alpha = 0.13$, and $\beta = 0.05$, respectively. All the constant control parameters were tuned via the Ziegler–Nichols method. The simulation results including output voltage, voltage control error, output currents, and current control error rates of the PDCC system using the 1PID and FB2PID control systems are shown in **FIGURE 8** and **FIGURE 9**, respectively. From the simulation results, both the output voltages were regulated to 48V through the proposed control scheme. Moreover, three converters were controlled by the 1PID and FB2PID control systems to share the output current equally. By comparing with the voltage and current errors as shown in **FIGURE 8** (b), (d) and **FIGURE 9** (b), (d), both the errors obtained by the 1PID control system were reduced by the FB2PID control system with regard to the additional compensation loop. Though the ACSC was achieved by the 1PID and FB2PID control systems, it cannot be ensured to perform the best control performance under the uses of the manually designed constant control parameters.

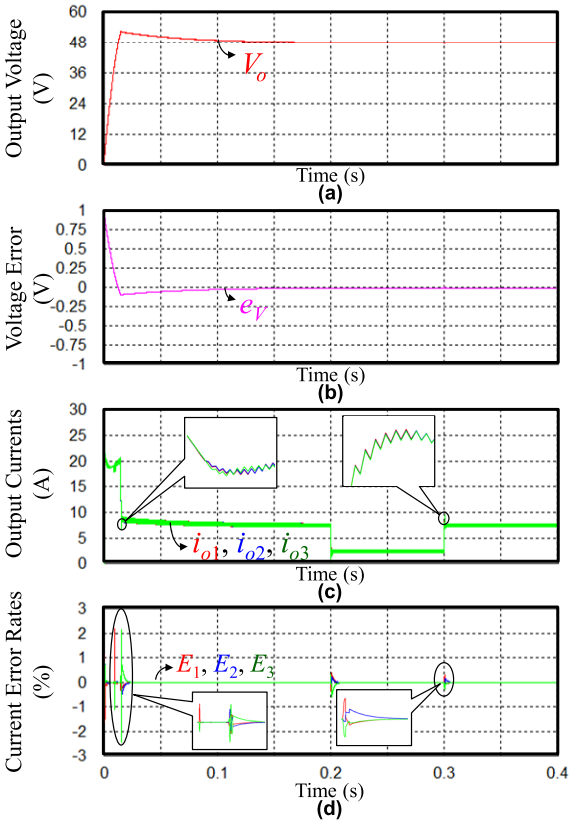

FIGURE 8. ACSC of the PDCC system using 1PID control system.

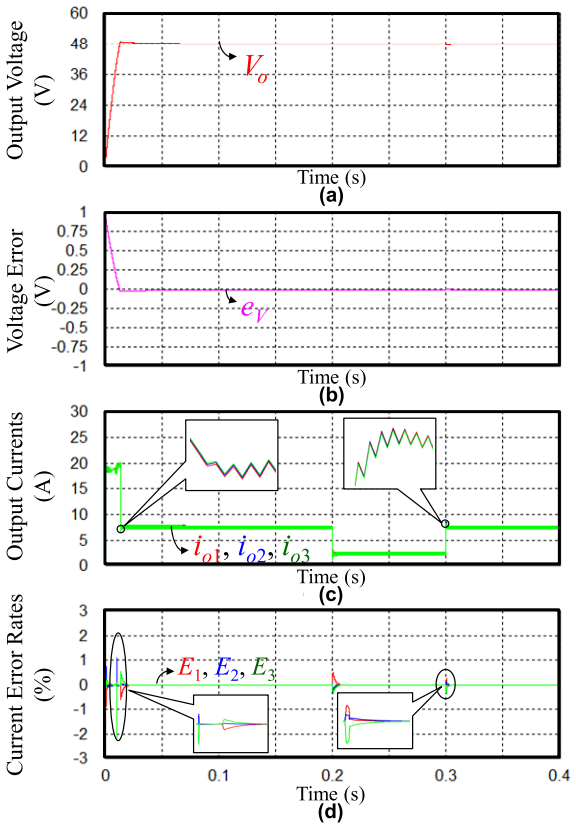

FIGURE 9. ACSC of the PDCC system using FB2PID control system.

The proposed BA-optimized FB2PID control system was applied to perform the ACSC of the PDCC system in which the control parameters of the FB2PID controllers in the inner current control loop were dynamically and concurrently optimized by the BA during the control process. The parameters for the BA were designed as $P = 5$, $\varphi = 0.9$, $\lambda = 0.85$, $f_{\min} = 0$, and $f_{\max} = 1$. Regarding the practical requirements, the search ranges for the control parameters were designed as $K_{Pi} \in [0.01, 10]$, $T_{Ii} \in [0.001, 1]$, $T_{Di} \in [0.001, 1]$, $\alpha_i \in [0.001, 1]$, and $\beta_i \in [0.001, 1]$, respectively. To show the evolutions of the BA-optimized control parameters, the changes of the first individual bat vector in the population with respect to the three converters are shown in **FIGURE 10** It is noted that all the values were normalized to [0, 1] for clear illustration. In the evolutions, all the bat vectors were initialized randomly and searched for the optimal solutions individually within the specific ranges. Moreover, the control parameters were updated every second. The effectiveness of the BA was demonstrated by the gradually increased fitness value as shown in **FIGURE 11**. After a number of 100 iterations, the fitness value was stable which indicates that the optimization was completed while the optimal control parameters were found. The simulation results of the PDCC system using the proposed BA-optimized FB2PID control system is shown in **FIGURE 12**. In the simulation, the control parameters of the K_{Pi}, T_{Ii}, T_{Di}, α_i, and β_i were eventually converged to 7.954, 0.1577, 0.103, 0.151, and 0.057 for the first converter, 7.992, 0.1575, 0.098, 0.149, and 0.047 for the second converter, and 8.026, 0.1571, 0.117, 0.149, and 0.062 for the third converter, respectively. The differences between the parameters imply that although the control objects are the same, the control parameter designs may still be slightly different due to the essential difference in the converter specifications. Compared with the ACSC using 1PID and FB2PID control systems with constant control parameters, three parallel-connected converters shared the load current more effectively by adopting the proposed BA-optimized FB2PID control system with online tuning control parameters. With respect to the high performance current control, the output voltage can also be regulated to 48V with faster response and lower overshoot.

The performance measures of the simulations are given for comparing the ACSC performances obtained by the 1PID, FB2PID, and the proposed BA-optimized FB2PID control systems in Table 2. By virtue of the online parameters optimization, the proposed BA-optimized FB2PID control system significantly improved the ACSC performance of the PDCC system. All the performance measures of the 1PID and FB2PID control systems were reduced by the BA-optimized FB2PID control system, as indicated in Table 2. The facts clearly reveal that the optimization and adaptiveness of the control parameters are able to enhance the ACSC performance and robustness.

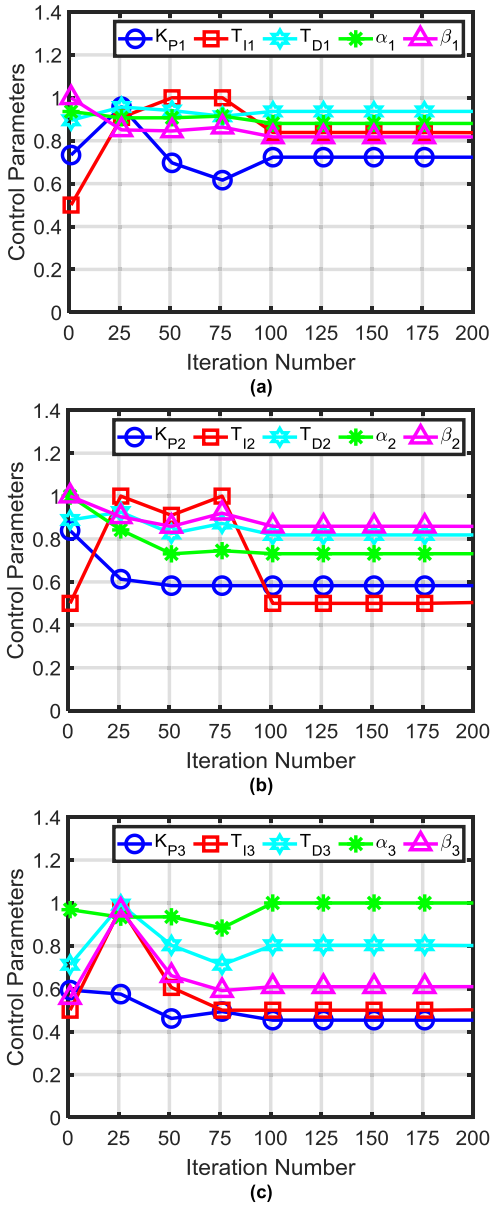

FIGURE 10. Evolutions of the control parameters of BA-optimized FB2PID controllers: (a) normalized values for the converter 1; (b) normalized values for the converter 2; (c) normalized values for the converter 3.

TABLE 2. Performance measures of the PDCC system with respect to the ACSC in simulation.

Control Loop	Items	1PID Control	FB2PID Control	BA-optimized FB2PID Control
Voltage Regulation Control (V)	P_{VM}	4.6085	1.1265	0.2458
	P_{VA}	0.7133	0.1402	0.0134
	P_{VS}	1.0399	0.2056	0.0156
Current Sharing Control (%)	P_{IM}	2.4231	2.1736	1.5674
	P_{IA}	0.0092	0.0072	0.0065
	P_{IS}	0.0666	0.0490	0.0420

VI. EXPERIMENTATION RESULTS

In this section, the ACSC performance and power transfer capability of the proposed PDCC system are investigated with

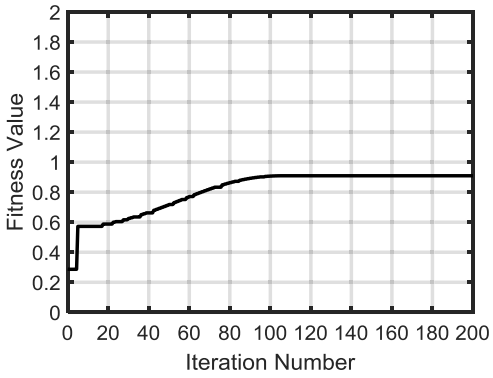

FIGURE 11. Evolutions of the fitness value optimized by BA.

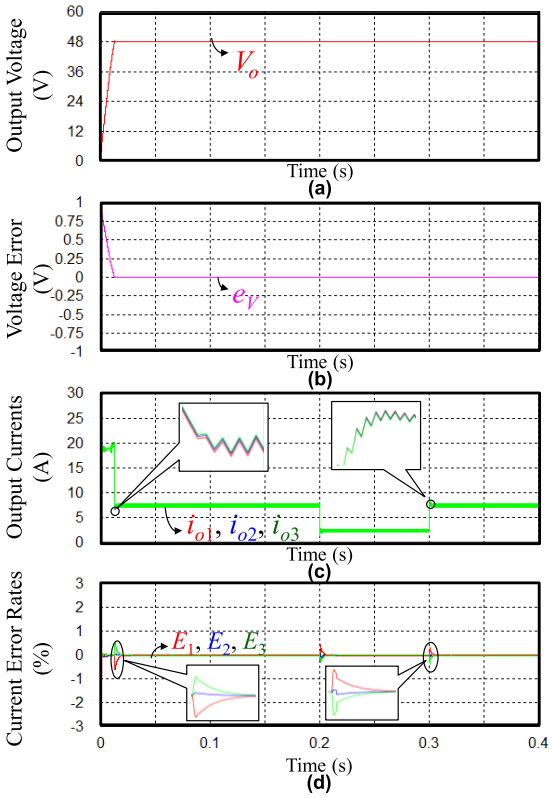

FIGURE 12. ACSC of the PDCC system using BA-optimized FB2PID control system.

experimental results. Experimental results of the proposed ACSC mechanism is realized with laboratory PDCC prototype as shown in **FIGURE 13**.

A. EXPERIMENTAL SETUP

To verify the effectiveness of the proposed ACSC scheme, a PDCC system containing three parallel-connected bi-directional converters was constructed and tested in this study. Each converter was developed with identical specification as provided in Table 3. According to the parallel-connected structure, the maximum output current and power of the PDCC system were increased to 60A and 3kW, respectively. In the experiments, three DC power supplies

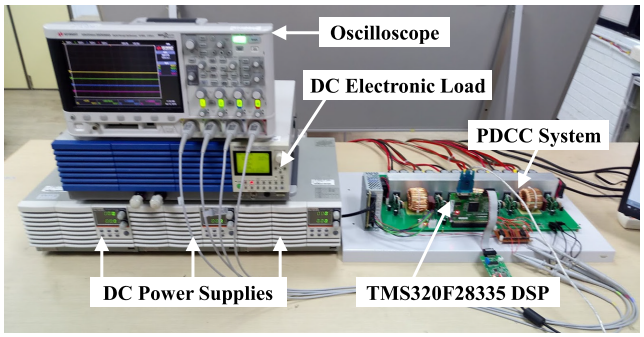

FIGURE 13. Experimental setup of the PDCC system.

TABLE 3. Specification of single DC/DC converter.

Item	Value
Input voltage (V)	0-100
Input current (A)	0-20
Rated power (W)	1 k
Inductance L (H)	300μ
Switching frequency f_s (Hz)	25 k
Capacitor C_1 and C_2 (F)	1000μ

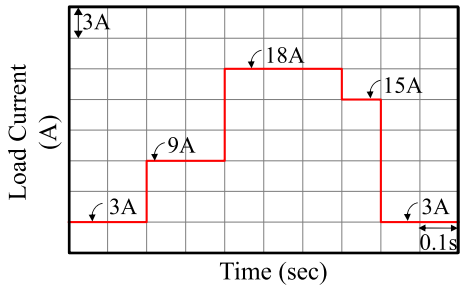

FIGURE 14. Designed time-varying load current of the PDCC system.

with output voltage 40V were used to provide the required power for the PDCC system. Moreover, the output voltage of the PDCC system was set as 48V so that the converters were operated at boost-discharging mode. A 32-bit floating-point TI TMS320F28335 DSP was the control core used to realize the proposed control strategies. In addition, a DC programmable electronic load was utilized to simulate a power load with several time-step changes as illustrated in **FIGURE 14**. The corresponding load power is 144, 432, 864, 720, and 144 W, respectively. The practical experimental setup is shown in **FIGURE 13**.

B. RESULTS

In the beginning of the experiments, the ACSC of the developed PDCC system was performed by using the 1PID and FB2PID control systems. The control parameters of the 1PID controllers were set to $K_P = 6.5$, $T_I = 0.02$, and $T_D = 0.2$ for the voltage control loop and $K_P = 1.5$, $T_I = 0.01$, and $T_D = 0.1$ for the current control loop, respectively. Besides, the constant parameters for the FB2PID controllers in the voltage and current control loops were chosen as $K_P = 8$,

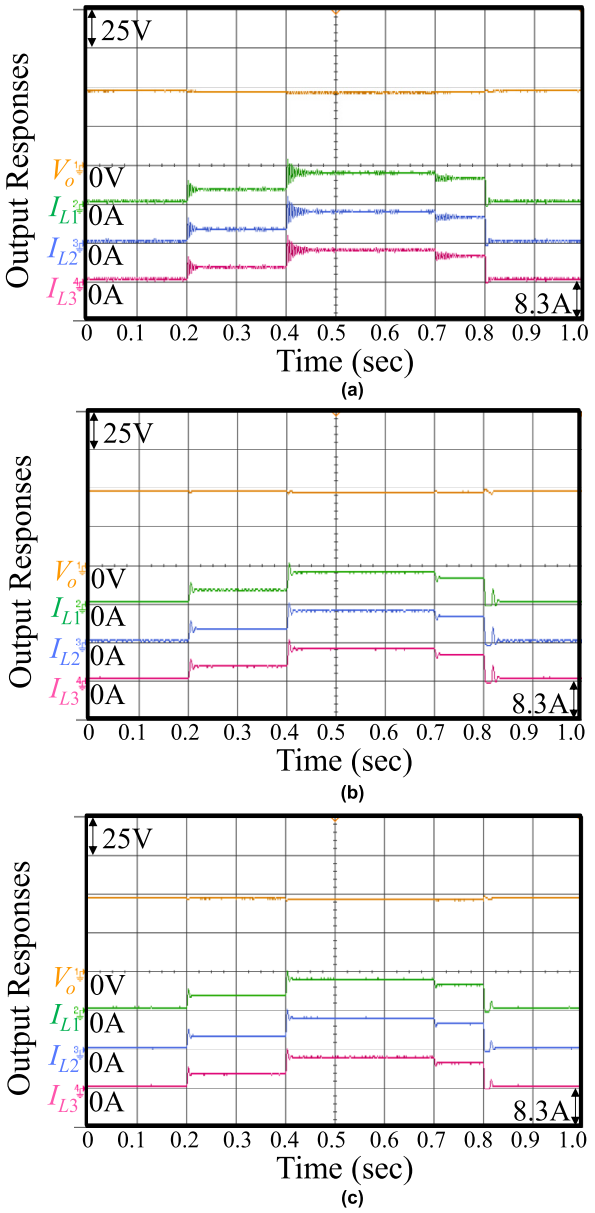

FIGURE 15. ACSC of the developed PDCC system using: (a) 1PID, (b) FB2PID, and (c) BA-optimized FB2PID control systems.

$T_I = 0.025$, $T_D = 0.3$, $\alpha = 0.5$, and $\beta = 0.2$, and $K_P = 1.6$, $T_I = 0.02$, $T_D = 0.1$, $\alpha = 0.5$, and $\beta = 0.2$, respectively. All the constant control parameters were tuned via the Ziegler–Nichols method. **FIGURE 15** (a) shows the experimental results of the ACSC obtained by the 1PID control system. According to the experimental results, the output voltage was regulated to 48V with obvious voltage vibrations. Though the output current of each converter was controlled to equally share the load current, the step responses of the current control such as overshoot, settling time, and steady-state error were not favorable due to the single control loop and constant control gains of the 1PID controller. In contrast, the FB2PID control system attenuated the chattering as seen in **FIGURE 15** (b). However, the robustness and transient response were evidently deteriorated at time-step

power changes. The limited control ability resulted from the constant control parameters is evident.

To improve the ACSC performance and robustness of the PDCC system under the time-varying load, the proposed BA-optimized FB2PID control system was used to control the output currents of the parallel-connected converters. The selection of the initial control parameters in the voltage and current control loops was referred to the FB2PID control system. They were dynamically optimized and updated during the experiment. The corresponding experimental results are shown in **FIGURE 15** (c). As opposed to the 1PID and FB2PID control systems, the ACSC performance of the PDCC system was considerably improved by using the proposed BA-optimized FB2PID control system. As a result, the control system integrating the online BA based tuning method and FB2PID control performs the best control performance compared with the conventional 1PID and FB2PID control systems. The performance measures of the experiments are summarized in Table 4. The best ACSC performances and robustness of the PDCC system using the proposed BA-optimized FB2PID control system under the occurrence of uncertainties can be clearly observed.

TABLE 4. Performance measures of the PDCC system with respect to the ACSC in experiments.

Control Loop	Items	1PID Control	FB2PID Control	BA-optimized FB2PID Control
Voltage Regulation Control (V)	P_{VM}	3.326	2.423	2.182
	P_{VA}	2.074	1.139	1.111
	P_{VS}	0.45	0.25	0.097
Current Sharing Control (%)	P_{IM}	100.065	22.292	5.955
	P_{IA}	6.329	2.082	1.749
	P_{IS}	7.367	2.115	0.828

VII. CONCLUSIONS

This study successfully presented an ACSC mechanism to actively balance the output currents of a PDCC system regarding the demanded power. In this study, the operating principle of the PDCC system was given first. Subsequently, a FB2PID control system was introduced to control the output voltage in DC bus and output current of each converter. To further improve the robustness of the current sharing performance of the FB2PID controlled PDCC system, a new BA-optimized FB2PID control system was proposed in which the control parameters in the current control loop were concurrently and dynamically optimized through a BA. As a result, the current control performances including transient and steady-state responses can be enhanced in the presence of uncertainties. Finally, simulation and experimental results demonstrated that the optimally designed BA-optimized FB2PID control system outperforms conventional 1PID and FB2PID control systems with regard to the PDCC system under time-varying load condition.

REFERENCES

[1] M. Li, C. K. Tse, H. H. C. Iu, and X. Ma, "Unified equivalent modeling for stability analysis of parallel-connected DC/DC converters," *IEEE Trans. Circuits Syst. II, Express Briefs*, vol. 57, no. 11, pp. 898–902, Nov. 2010.

[2] D. Sha, J. Zhang, X. Wang, and W. Yuan, "Dynamic response improvements of parallel-connected bidirectional DC–DC converters for electrical drive powered by low-voltage battery employing optimized feedforward control," *IEEE Trans. Power Electron.*, vol. 32, no. 10, pp. 7783–7794, Oct. 2017.

[3] S. K. Mazumder, M. Tahir, and K. Acharya, "Master–Slave current-sharing control of a parallel DC–DC converter system over an RF communication interface," *IEEE Trans. Ind. Electron.*, vol. 55, no. 1, pp. 59–66, Jan. 2008.

[4] Y. M. Lai, S. C. Tan, and Y. M. Tsang, "Wireless control of load current sharing information for parallel-connected DC/DC power converters," *IET Power Electron.*, vol. 2, no. 1, pp. 14–21, Jan. 2009.

[5] Z. Chen, Y.-N. Guo, M. Chen, and L. Ge, "Study on PI sliding mode controller for paralleled dc-dc converter," in *Proc. IEEE 8th Int. Power Electron. Motion Control Conf.*, Hefei, China, May 2016, pp. 3079–3083.

[6] H. Du, C. Jiang, G. Wen, W. Zhu, and Y. Cheng, "Current sharing control for parallel DC–DC buck converters based on finite-time control technique," *IEEE Trans. Ind. Inform.*, vol. 15, no. 4, pp. 2186–2198, Apr. 2019.

[7] U. B. Tayab, M. A. Roslan, L. J. Hwai, and M. Kashif, "A review of droop control techniques for microgrid," *Renewable Sustain. Energy Rev.*, vol. 76, pp. 717–727, Sep. 2017.

[8] C. Wu, B. Lu, and Y. Ge, "A novel parallel current-sharing control method of switch power supply," *Open Elect. Electron. Eng. J.*, vol. 8, pp. 170–177, Aug. 2014.

[9] S. Ali, T. Shengxue, Z. Jianyu, A. Ali, and A. Nawaz, "An implementation of parallel buck converters for common load sharing in DC microgrid," *Information*, vol. 10, no. 3, p. 91, Mar. 2019.

[10] J. B. Wang, "Parallel DC/DC converters system with a novel primary droop current sharing control," *IET Power Electron.*, vol. 5, no. 8, pp. 1569–1580, Sep. 2012.

[11] X. Lu, J. M. Guerrero, K. Sun, and J. C. Vasquez, "An improved droop control method for dc microgrids based on low bandwidth communication with dc bus voltage restoration and enhanced current sharing accuracy," *IEEE Trans. Power Electron.*, vol. 29, no. 4, pp. 1800–1812, Apr. 2014.

[12] H.-C. Chiang, K. K. Jen, and G.-H. You, "Improved droop control method with precise current sharing and voltage regulation," *IET Power Electron.*, vol. 9, no. 4, pp. 789–800, Mar. 2016.

[13] S. Augustine, M. K. Mishra, and N. Lakshminarasamma, "Adaptive droop control strategy for load sharing and circulating current minimization in low-voltage standalone DC microgrid," *IEEE Trans. Sustain. Energy*, vol. 6, no. 1, pp. 132–141 , Jan. 2015.

[14] T. V. Vu, D. Perkins, F. Diaz, D. Gonsoulin, C. S. Edrington, and T. EI-Mezyani, "Robust adaptive droop control for DC microgrids," *Electr. Power Syst. Res.*, vol. 146, pp. 95–106, May 2017.

[15] S. Golshannavaz and V. Morteznpour, "A generalized droop control approach for islanded DC microgrids hosting parallel-connected DERs," *Sustain. Cities Soc.*, vol. 36, pp. 237–245, Jan. 2018.

[16] K. W. Lao, N. Dai, and J. Sheng, "An improved closed-loop droop control technique for higher utilization of power output capability in CCI," *Int. J. Electr. Power Energy Syst.*, vol. 109, pp. 455–469, Jul. 2019.

[17] S. Luo, Z. Ye, R.-L. Lin, and F. C. Lee, "A classification and evaluation of paralleling methods for power supply modules," in *Proc. 30th Annu. IEEE Power Electron. Spec. Conf.*, Charleston, SC, USA, Jul. 1999, pp. 901–908.

[18] M. L. Bolloch, M. Cousineai, and T. Meynard, "New masterless modular current-sharing technique for DC/DC parallel converters," in *Proc. 14th Int. Power Electron. Motion Control Conf.*, Sep. 2010, pp. T3-73–T3-80.

[19] Y. Kanthaphayao and V. Chunkag, "Current-sharing bus and fuzzy gain scheduling of proportional-integral controller to control a parallel-connected AC/DC converter," *IET Power Electron.*, vol. 7, no. 10, pp. 2525–2532, Oct. 2014.

[20] R. Long, Shuhai. Quan, L. Zhang, Q. Chen, C. Zeng, and L. Ma, "Current sharing in parallel fuel cell generation system based on model predictive control," *Int. J. Hydrogen Energy*, vol. 40, no. 35, pp. 11587–11594, Sep. 2015.

[21] C.-H. Cheng, P.-J. Cheng, and M.-J. Xie, "Current sharing of paralleled DC–DC converters using GA-based PID controllers," *Expert Syst. Appl.*, vol. 37, no. 1, pp. 733–740, Jan. 2010.

[22] D. Fister, I. Fister, Jr, I. Fister, and R. Šafarič, "Parameter tuning of PID controller with reactive nature-inspired algorithms," *Robot. Auto. Syst.*, vol. 84, pp. 64–75, Oct. 2016.

[23] H. Habibi, H. R. Nohooji, and I. Howard, "Adaptive PID control of wind turbines for power regulation with unknown control direction and actuator faults," *IEEE Access*, vol. 6, pp. 37464–37479, 2018.

[24] B. Verma and P. K. Padhy, "Optimal PID controller design with adjustable maximum sensitivity," *IET Control Theory Appl.*, vol. 12, no. 8, pp. 1156–1165, May 2018.
[25] S.-Y. Chen, C.-S. Chen, and Z.-W. Yang, "Self-tuning cross-coupled two degree-of-freedom PID control for position synchronization of dual linear motors," *Appl. Math. Model.*, vol. 64, pp. 214–234, Dec. 2018.
[26] Z. Pan, F. Dong, J. Zhao, L. Wang, H. Wang, and Y. Feng, "ombined resonant controller and two-degree-of-freedom PID controller for PMSLM current harmonics suppression," *IEEE Trans. Ind. Electron.*, vol. 65, no. 9, pp. 7558–7568, Sep. 2018.
[27] M. Kumar and V. V. Patel, "Tuning of two degree of freedom PID controller for second order processes," *Int. J. Sci., Eng. Technol. Res.*, vol. 4, no. 5, pp. 1543–1546, Jan. 2015.
[28] V. M. Alfaro and R. Vilanova, "Robust tuning of 2DoF five-parameter PID controllers for inverse response controlled processes," *J. Process Control*, vol. 23, no. 4, pp. 453–462, Apr. 2013.
[29] J. R. Lagunas-Jiménez, V. Moo-Yam, and B. Ortíz-Moctezuma, "Two-degrees-of-freedom robust PID controllers tuning via a multiobjective genetic algorithm," *Computacion y Sist.*, vol. 18, no. 2, pp. 259–273, Jun. 2014.
[30] A. R. Meena and S. S. Kumar, "Design of GA tuned two-degree freedom of PID controller for an interconnected three area automatic generation control system," *Indian J. Sci. Technol.*, vol. 8, no. 12, pp. 1–10, Jun. 2015.
[31] K. Sundaravadivu, S. Sivakumar, and N. Hariprasad, "2DOF PID controller design for a class of FOPTD models—An analysis with heuristic algorithms," *Procedia Comput. Sci.*, vol. 48, pp. 90–95, Aug. 2015.
[32] A. Chakri, R. Khelif, M. Benouaret, and X.-S. Yang, "New directional bat algorithm for continuous optimization problems," *Expert Syst. Appl.*, vol. 69, pp. 159–175, Mar. 2017.
[33] A. Slowik and H. Kwasnicka, "Nature inspired methods and their industry applications-swarm intelligence algorithms," *IEEE Trans. Ind. Inform.*, vol. 14, no. 3, pp. 1004–1015, Mar. 2018.
[34] M. S. B. Ameur and A. Sakly, "FPGA based hardware implementation of bat algorithm," *Appl. Soft Comput.*, vol. 58, pp. 378–387, Sep. 2017.
[35] M. A. Al-Betar, M. A. Awadallah, H. Faris, X.-S. Yang, A. T. Khader, and O. A. Alomari, "Bat-inspired algorithms with natural selection mechanisms for global optimization," *Neurocomputing*, vol. 273, pp. 448–465, Jan. 2018.
[36] M. A. Al-Betar and M. A. Awadallah, "Island bat algorithm for optimization," *Expert Syst. Appl.*, vol. 107, pp. 126–145, Oct. 2018.
[37] A. Aggarwal, T. K. Rawat, and D. K. Upadhyay, "Optimal design of L_1-norm based IIR digital differentiators and integrators using the bat algorithm," *IET Signal Process.*, vol. 11, no. 1, pp. 26–35, Feb. 2016.
[38] J. Senthilnath, S. Kulkarni, J. A. Benediktsson, and X. S. Yang, "A novel approach for multispectral satellite image classification based on the bat algorithm," *IEEE Geosci. Remote Sens. Lett.*, vol. 13, no. 4, pp. 599–603, Apr. 2016.
[39] H.-C. Huang, "Fusion of modified bat algorithm soft computing and dynamic model hard computing to online self-adaptive fuzzy control of autonomous mobile robots," *IEEE Trans. Ind. Inform.*, vol. 12, no. 3, pp. 972–979, Jun. 2016.
[40] H. Dehghani and D. Bogdanovic, "Copper price estimation using bat algorithm," *Resour. Policy*, vol. 55, pp. 55–61, Mar. 2018.
[41] P. Savsani, R. L. Jhala, and V. J. Savsani, "Comparative study of different metaheuristics for the trajectory planning of a robotic arm," *IEEE Syst. J.*, vol. 10, no. 2, pp. 697–708, Jun. 2016.
[42] A. Kavousi-Fard, A. Khosravi, and S. Nahavandi, "A new fuzzy-based combined prediction interval for wind power forecasting," *IEEE Trans. Power Syst.*, vol. 31, no. 1, pp. 18–26, Jan. 2016.
[43] T. Y. Tan, L. Zhang, C. P. Lim, and B. Fielding, "Evolving ensemble models for image segmentation using enhanced particle swarm optimization," *IEEE Access*, vol. 7, pp. 34004–34019, Mar. 2019.
[44] A. E. Ezugwu and F. Akutsah, "An improved firefly algorithm for the unrelated parallel machines scheduling problem With sequence-dependent setup times," *IEEE Access*, vol. 6, pp. 54459–54478, 2018.
[45] A. M. Abdelbar and K. M. Salama, "Parameter self-adaptation in an ant colony algorithm for continuous optimization," *IEEE Access*, vol. 7, pp. 18464–18479, 2019.
[46] K. B. Liu, C. Y. Liu, Y. C. Chien, B. S. Wang, Y. S. Wong, and Y. H. Liu, "Analysis and controller design of a universal bidirectional DC–DC converter," *Energies*, vol. 9, no. 7, pp. 501–523, Jun. 2016.

SYUAN-YI CHEN received the Ph.D. degree in electrical engineering from National Central University, Taiwan, in 2010. From 2010 to 2013, he was an R&D Engineer and the Project Leader with Information and Communications Research Laboratories, Industrial Technology Research Institute, Hsinchu, Taiwan. From 2014 to 2017, he was an Assistant Professor with the Department of Electrical Engineering, National Taiwan Normal University, Taipei, Taiwan, where he is currently an Associate Professor. His main research interests include nonlinear and intelligent control, machine learning and artificial intelligence, and vehicle power management and control.

BO-CHEN YANG received the M.S. degree in electrical engineering from National Taiwan Normal University, Taipei, Taiwan, in 2018. Since 2018, he has been an Engineer with the Power Design Department I, Wistron Corporation, Taiwan. His research interests include power electronics, active current-sharing control, and optimization theories.

TSE-AN PU received the B.S. degree in electrical engineering from Chung Hua University, Hsinchu, Taiwan, in 2017. He is currently pursuing the M.S. degree in electrical engineering with National Taiwan Normal University, Taipei, Taiwan. His research interests include vehicle power management systems, fuel cell electric vehicle control, and power conversion systems.

CHIH-HUNG CHANG received the B.S. degree in electrical engineering from the Lee-Ming Institute of Technology, New Taipei City, Taiwan, in 2013. He is currently pursuing the M.S. degree in electrical engineering with National Taiwan Normal University, Taipei, Taiwan. His research interests include microgrid, smart home energy management systems, and power conversion systems.

RUEI-CING LIN received the B.S. degree in electrical engineering from National Taiwan Normal University, Taipei, Taiwan, in 2018, where he is currently pursuing the M.S. degree. His research interests include evolutionary algorithm, hybrid electric vehicle control, and vehicle power management systems.